Ferromagnetism in oxide semiconductors

Over the past five years, considerable work has been carried out in the exploration of candidate diluted oxide magnetic semiconductors with high Curie temperatures. Fueled by early experimental results and theoretical predictions, claims of ferromagnetism at and above room temperature in doped oxides have abounded. In general, neither the true nature of these materials nor the physical causes of the magnetism have been adequately determined. It is now apparent that these dilute magnetic systems are deceptively complex. We consider two well-characterized n-type magnetically doped oxide semiconductors and explore the relationship between donor electrons and ferromagnetism.

S. A. Chambers[1*], T. C. Droubay[1], C. M. Wang[1], K. M. Rosso[1], S. M. Heald[2], D. A. Schwartz[3], K. R. Kittilstved[3], and D. R. Gamelin[3]

[1]Fundamental Science Directorate, Pacific Northwest National Laboratory, Richland, WA USA

[2]Advanced Photon Source, Argonne National Laboratory, Argonne, IL USA

[3]Department of Chemistry, University of Washington, Seattle, WA USA

**E-mail: sa.chambers@pnl.gov*

In order to become a practical technology, semiconductor spintronics requires the discovery and use of ferromagnetic semiconductors that exhibit spin polarization in the majority carrier band at and above room temperature. Intrinsic remanent magnetization would allow spin-polarized currents to propagate in such materials without the need for a continuous magnetic field.

However, the discovery and understanding of such materials is proving to be a grand challenge in solid-state science. Indeed, one of the 125 critical unanswered scientific questions recently posed in *Science*[1] asks, "Is it possible to create magnetic semiconductors that work at room temperature?" The materials challenge is great because both magnetic and electronic doping is required, and the interaction between magnetic dopant spins and free carriers must be engineered to achieve thermally robust dopant spin-carrier coupling. The magnetic dopant must have unpaired *d* electrons in order to exhibit a net spin. The ferromagnetic alignment of these spins throughout the material is brought about by the spin polarization of and interaction with free carriers. After poling to saturation with an external magnetic field, remanent magnetization of the dopant spins at zero field is retained via spin-polarized carriers. The associated spin-polarized current is what gives spintronic devices their new and novel functionality. In some cases, such as Mn:GaAs, the magnetic and electronic dopants are the same species. In other cases, such as Co:ZnO, the magnetic dopant does not provide carriers, and an electronic dopant must be added.

The most thoroughly studied and best understood ferromagnetic semiconductor, Mn:GaAs, suffers from a loss of magnetization at

ISSN:1369 7021 © Elsevier Ltd 2006

temperatures above 170 K[2]. Although well below room temperature, a Curie point of 170 K is still quite high for carrier-mediated ferromagnetism, based on our understanding of the process. However, because of this practical limitation, materials scientists are motivated to find other magnetic semiconductors that are more thermally robust. The most flexible and ultimately useful approach to synthesizing ferromagnetic semiconductors is to dope nonmagnetic semiconductors with transition metals containing unpaired *d* electrons. Such materials are known as diluted magnetic semiconductors (DMS). The ferromagnetism in DMS materials is in principle tunable and gateable.

Several years ago, Dietl *et al.*[3,4] predicted on the basis of mean field theory that a few relatively low atomic number DMS materials ($Mn_{0.05}Ga_{0.95}N$, $Mn_{0.05}Zn_{0.95}O$, and $Mn_{0.025}C_{0.975}$) should exhibit above-room-temperature ferromagnetic ordering of the Mn dopants mediated by additional holes, assumed to be present at a concentration of 3.5×10^{20} cm^{-3}.

As a result of these calculations, experimentalists on every continent have grown films of GaN and ZnO doped with every first-row transition metal element to see if any of these combinations exhibit room temperature ferromagnetism (RTFM). These studies have frequently been marked by inadequate attention to detail and quality in film growth and characterization, and many unsubstantiated claims of success have been made in the literature, particularly for ZnO. Moreover, the mechanism(s) of magnetism are still not adequately understood. (The reader is referred elsewhere[5-9] for a more complete discussion of this literature.) As a result, the experimental results for Mn:ZnO are still largely inconclusive. Moreover, the problem is exacerbated by the fact that it is difficult to dope ZnO *p*-type. Unintended donors that originate from several common impurities and defects can compensate holes[10]. Without being able to achieve *p*-type doping, it is not possible to test directly the predictions of Dietl *et al.*[3,4] concerning Mn:ZnO.

Although transport studies that convincingly demonstrate *p*-type conductivity in Mn:ZnO have not been done, less direct spectroscopic studies have been carried out with encouraging results. Kittilstved *et al.*[11] made Mn:ZnO films by spin coating Mn:ZnO nanoparticles capped with a N-containing ligand[12] and performed optical absorption measurements. These studies reveal that occupied Mn *d* states in the ZnO band gap hybridize with holes from the surface-bound N, leading to the resonance $Mn(III) \times Mn(II) + h^{+}_{VB}$. This interaction would seem to *require* holes to mediate ferromagnetic exchange coupling between Mn dopants in Mn:ZnO effectively, although the possibility that bound magnetic polarons associate with localized holes resulting from N dopants in *n*-type (Mn,N):ZnO cannot be dismissed[13].

Another prediction from Dietl's calculations[3,4] is that αN_o, the *s-d* exchange energy that parameterizes the interaction of dopant *d* electrons with the *s*-derived conduction band of the host semiconductor, is sufficiently weak that RTFM is not expected for magnetically doped *n*-type ZnO or GaN. It is therefore of interest to search for a magnetic dopant that would effectively couple to donor states and probe the thermal robustness of such a material.

Early density functional theory (DFT) calculations by Sato and Katayama-Yoshida[14] predict that Co may be such a magnetic dopant. Additionally, spectroscopic studies of Co:ZnO nanoparticle films impregnated with interstitial Zn (Zn_i), a shallow donor, reveal that the resonance $Co(I) \leftrightarrow Co(II) + e^{-}_{CB}$ is energetically favorable[11,12,15]. Therefore, *n*-type Co:ZnO may constitute an intriguing prototypical system to investigate the efficacy of donors in activating RTFM in magnetically doped ZnO.

In this brief review, we discuss two doped transition metal epitaxial oxides that we have studied in some detail (Co:ZnO and Ti:α-Fe_2O_3) and investigate the possibility of room temperature electron-mediated ferromagnetic exchange in these materials. These two systems were picked because although they are relatively lightly studied in the literature, very recent work in our laboratory shows they are good candidates for investigating the interaction between donor electrons from the electronic dopant and magnetic dopant spins. We show that the saturation moment at 300 K in Co:ZnO is correlated with the presence of donor electrons from Zn_i, which is diffused into the lattice after growth. In Ti:Fe_2O_3, Ti acts as both a donor and a magnetic 'undopant'[16]. Ti(IV), a d^0 cation, displaces Fe(III) spins in the antiferromagnetic host lattice, resulting in a net magnetization at 300 K. Carriers are also generated by the Ti dopants, but we show that the saturation magnetization is independent of carrier concentration.

Co-doped ZnO

An ideal way to demonstrate carrier-mediated ferromagnetism in ZnO is to fabricate a spin light-emitting diode (spin-LED). ZnO is a strong light emitter in the ultraviolet, and electron-hole pair recombination in a quantum well in which at least one kind of carrier is spin polarized should lead to circularly polarized light emission with the optical polarization being equal to the spin polarization[17-19]. However, such a device requires the ability to grow both *n*- and *p*-type ZnO, and *p*-type material is difficult to grow. Indeed, initial attempts to fabricate a spin-LED using (Mn,Sn):ZnO, which is nominally *n*-type, as the spin injector resulted in negligible (less than ~10%) circular polarization, even at very low temperatures (2 K) and high magnetic field (4 T)[20]. Thus, until the *p*-type doping problem is solved, another approach must be taken.

One such approach is to demonstrate that the observation of RTFM in Co:ZnO is correlated with the presence of donor electrons in a quantitative way. To this end, Schwartz and Gamelin[21] have taken epitaxial films of Co:ZnO grown on α-Al_2O_3(012) by metal organic chemical vapor deposition by Tuan *et al.*[22] and have diffused in atomic Zn. The specimens consist of single-crystal films in which Co(II) substitutes for Zn(II) in the lattice, as evidenced by Co 2*p* X-ray photoelectron, Co K-shell X-ray absorption, and optical absorption spectroscopies. In-diffused Zn occupies interstitial sites and acts as a

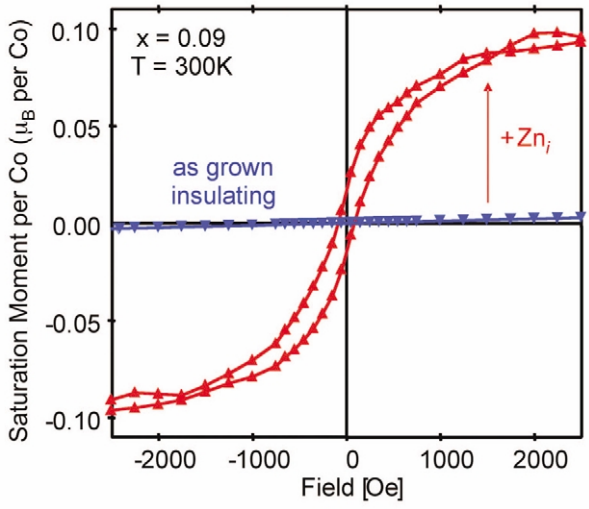

Fig. 1 In-plane magnetic hysteresis loops for epitaxial $Zn_{0.09}Co_{0.91}O/\alpha$-$Al_2O_3(012)$ before and after Zn indiffusion and the resulting conversion from insulating to n-type, measured at 300 K.

shallow donor in ZnO, as evidenced by a strong near-infrared absorption assigned to the intra-conduction-band excitation of free or shallow-bound electrons in ZnO[23]. This process converts $Co_{0.09}Zn_{0.91}O$ from being insulating and paramagnetic to being semiconducting and slightly ferromagnetic, as seen in Fig. 1[12,21]. The 300 K saturation moment (~0.1 Bohr magnetons per Co, or μ_B/Co) is considerably less than that expected for Co(II) in tetrahedral coordination (~3 μ_B/Co). However, 0.1 μ_B/Co is reasonable in light of the small ratio of donor electrons from Zn$_i$ to Co (~1:100), if indeed the ferromagnetism is carrier mediated.

Fig. 2a shows the effect of Zn indiffusion and air annealing on in-plane saturation magnetization at room temperature, conductivity, and Co *d*-to-*d* ligand field (LF) absorbance over several cycles[12,21]. The air anneal removes Zn$_i$, presumably by drawing Zn$_i$ out to the surface, oxidizing it, and depositing new surface layers of pure ZnO. The saturation magnetization and conductivity track together in a fully reversible fashion. Moreover, these are out of phase with the Co LF optical absorption, which is characteristic of paramagnetic Co(II) in tetrahedral coordination and is therefore most intense when the Co paramagnetic fraction is maximized. This result unambiguously

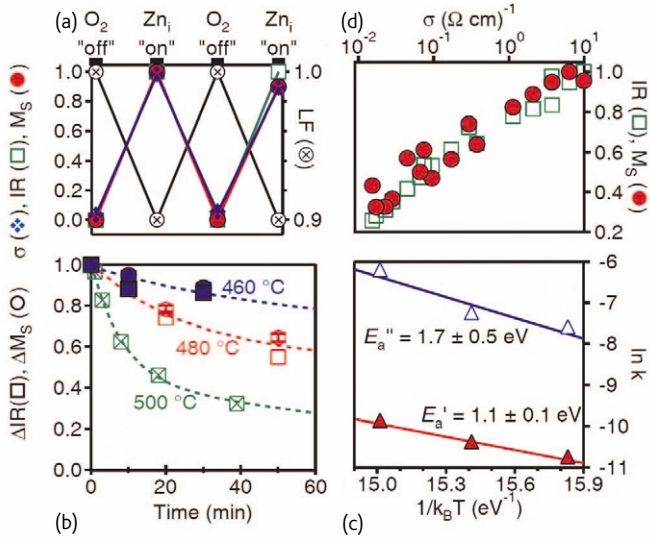

Fig. 2 (a) Quantitatively reversible cycling of the room-temperature saturation magnetization M_S (red circle), conductivity σ (blue diamond), infrared (IR) absorbance (green square), and LF absorption (crossed circle) for epitaxial $Zn_{0.09}Co_{0.91}O$ with alternating air (off) and Zn vapor (on) annealing. (b) Kinetic decay curves for room temperature M_S (circles) and IR intensities (square) versus oxidation time at 460°C, 480°C, and 500°C. Best fit double-exponential decay curves are shown as dashed lines. (c) Natural logs of the two rate constants versus inverse thermal energy. The linear slopes yield the activation energies indicated. (d) Room temperature M_S and IR absorbance versus the log of the conductivity at room temperature for data from (b).

demonstrates a correlation between ferromagnetism and conductivity. To further verify that the ferromagnetism is directly correlated with the donor electron concentration, Kittilstved *et al.*[24] have measured the kinetics of the ferromagnetic-to-paramagnetic phase transition and the semiconductor-to-insulator transition as a (Zn_i,Co):ZnO epitaxial film is annealed in air. The initial decay curves for the saturation moment and near infrared absorption are shown in Fig. 2b at different temperatures. The two physical properties are clearly correlated, both showing similar double exponential decay kinetics that track together as temperature is elevated. Such a correlation can only occur if the ferromagnetism and infrared absorption are associated with the same species, namely Zn_i. Activation energies for Zn_i diffusion can be obtained via Arrhenius plots, as seen in Fig. 2c and discussed below. Furthermore, when the data from Fig. 2b are plotted versus the film conductivity on a logarithmic scale, a clear linear relationship is observed for both saturation moment and IR absorption, as seen in Fig. 2d. Combined, these data clearly demonstrate a direct correlation between ferromagnetism and Zn_i-derived carriers in Co:ZnO.

Fig. 2c plots the fast and slow decay rate constants from the data in Fig. 2b versus the inverse thermal energy for the different oxidation temperatures. Straight lines are obtained, indicating Arrhenius behavior. Two activation energies are extracted for oxidative quenching of ferromagnetism, $E_a' = 1.1 \pm 0.1$ eV and $E_a'' = 1.7 \pm 0.5$ eV. These values are comparable to those reported for the diffusion of Zn_i in ZnO, which range from 0.87 eV to 1.52 eV for temperatures between 375°C and 940°C[25-27]. The two activation barriers may be related to Zn_i diffusion through the lattice and more rapid diffusion along grain boundaries, both leading to rapid oxidation at the ZnO/air interface. These low activation barriers are consistent with diffusion of Zn_i (a non-Frenkel lattice defect) but not with diffusion of oxygen vacancies (V_O), which requires displacement of substitutional anions. Literature activation energies for oxygen diffusion in ZnO are much larger than those in Fig. 2c (e.g. >5.0 eV for bulk ZnO, ~3.1 eV for polycrystalline ZnO, and ~3.4 eV for polycrystalline Co:ZnO[28]). The data in Fig. 2 thus provide strong evidence that Zn_i, and not V_O, is the defect responsible for the ferromagnetism in Co:ZnO described here. However, a nonzero saturation moment remains even when the conductivity becomes so low that the material can no longer be considered a doped semiconductor, as seen in Fig. 2d. Therefore, delocalized free carriers and metallic conductivity are not required for RTFM in Co:ZnO. Hence this ferromagnetism does not arise entirely from the Ruderman-Kittel-Kasuya-Yoshida (RKKY) mechanism often applied to ferromagnetic semiconductors. In the RKKY mechanism, the itinerant carrier gas is polarized by the magnetic dopant spins even when the latter are present as a dilute species[29]. When the magnetic field is removed, remanent spin polarization remains in place, unless the carriers are swept out, in which case the magnetization goes to zero. Rather, the data in Fig. 2 support a description of ferromagnetism in (Zn_i,Co):ZnO also involving bound magnetic polarons[28,30,31]. Here, shallow bound donor electrons associated with Zn_i occupy orbitals that are sufficiently spatially diffuse such that they overlap with and magnetically align multiple Co dopants. Mutual overlap of such polaronic states results in macroscopic ferromagnetism, even in the absence of measurable conductivity.

To further demonstrate that there is a direct correlation between the observed ferromagnetic response at room temperature and

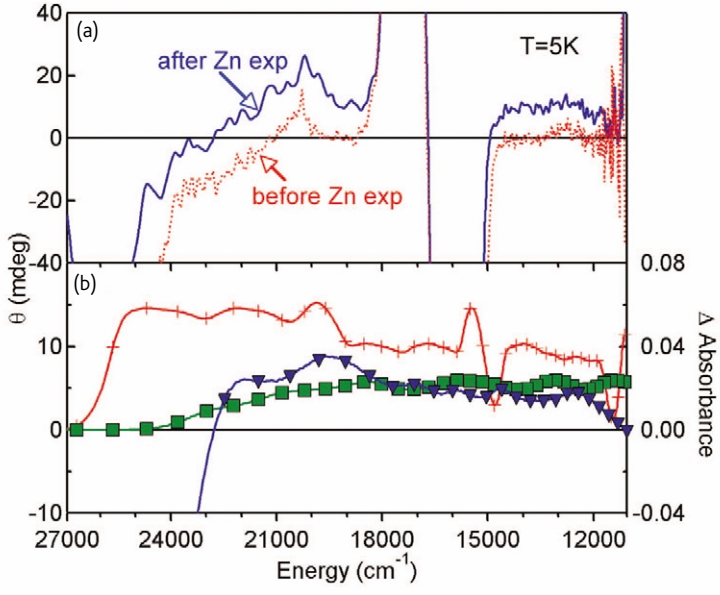

Fig. 3 (a) Optical magnetic circular dichroism for epitaxial $Zn_{0.09}Co_{0.91}O$ before and after Zn indiffusion, measured at 5 K at 6.5 T. (b) Dichroism at zero field at 5 K (red plus sign) and 300 K (green square), along with the difference in optical absorbance between the ferromagnetic and paramagnetic states of the film at 300 K (blue triangle).

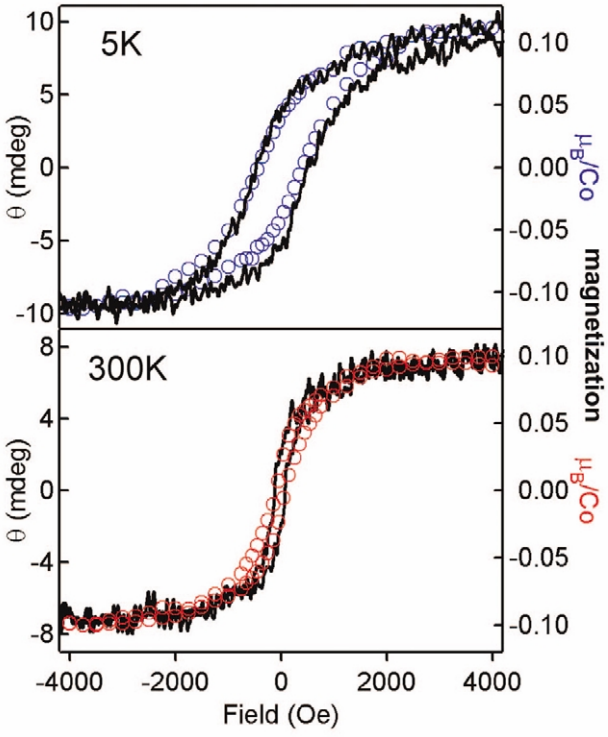

Fig. 4 In-plane magnetic hysteresis loops extracted from dichroism spectra (solid curves) and superconducting quantum interference device (SQUID) loops (circles) for epitaxial $Zn_{0.09}Co_{0.91}O$ at 5 K and 300 K.

Zn_i-derived donor electrons, we point to the effect of Zn_i on the optical magnetic circular dichroism (MCD). Before Zn exposure, the MCD increases with magnetic field in a way consistent with Brillouin paramagnetism, and is strongly temperature dependent[22]. After Zn exposure, the MCD changes substantially, as seen in Fig. 3a. Over the paramagnetic MCD a broad new MCD feature is superimposed that is nearly temperature independent. This feature is assigned to excitations from a new state resulting from hybridization of the Co *d* states at the top of the gap and shallow donor states from Zn_i. There is no MCD at all for pure ZnO, establishing that the dichroism is caused by the Co dopant. Fig. 3b shows the *remanent* dichroism at 5 K and 300 K, along with the difference in absorbance between ferromagnetic and paramagnetic states of Co:ZnO at 300 K. This result is remarkable in that it shows a substantial dichroic effect at zero field *and* 300 K across the $^4A_2(F) \rightarrow {}^4T_1(P)$ ligand-field absorption band associated with Co(II) in tetrahedral coordination, thereby linking the ferromagnetism to the substitutional magnetic dopant. From the data in Fig. 3a, we can construct magnetic hysteresis loops for the Zn-diffused Co:ZnO, and these are shown in Fig. 4. Here we plot the dichroism at 14 250 cm^{-1} at 5 K and 300 K as a function of field strength and overlap these with the associated in-plane magnetization loops. This frequency is well within the broad absorbance and dichroism bands assigned to the Zn_i donor-Co 3*d* hybridized state. There is good overlap between the two hysteresis loops at each temperature, establishing that the ferromagnetic response is clearly the a result of the *simultaneous* presence of Co dopants and shallow donors from Zn_i.

Ti-doped α-Fe_2O_3

We now examine the role of carriers in the magnetism of Ti:α-Fe_2O_3. High-quality, single-crystal films of Ti:α-Fe_2O_3 were grown by oxygen-plasma-assisted molecular beam epitaxy on α-Al_2O_3(001). A buffer layer of α-Cr_2O_3 was first grown to take up the strain created by the large in-plane lattice mismatch between α-Al_2O_3 and α-Fe_2O_3[32]. Ti serves the dual role of electronic and magnetic dopant. Ti(IV) substitutes for Fe(III) in the lattice. Fig. 5 shows the Ti K-shell X-ray absorption near-edge structure along with the measured and simulated extended fine structure. Comparison of the near-edge structure with appropriate standards (Fig. 5a) reveals that Ti is formally Ti(IV). Fourier transforms of the extended fine structure are very well simulated assuming Ti substitution for Fe, as seen for $x = 0.04$ in Fig. 5b. Therefore, Ti should be a donor in Fe_2O_3. However, Ti can also be

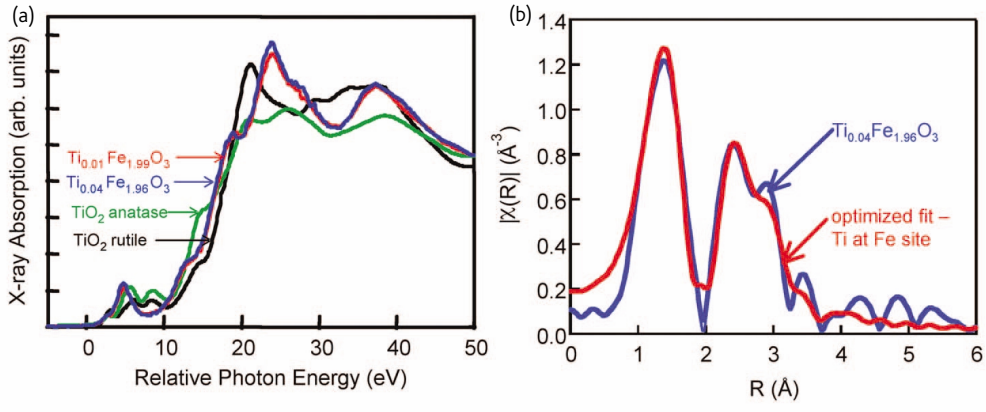

Fig. 5 (a) Ti K-shell X-ray absorption near-edge spectra for $Ti_xFe_{2-x}O_3$ epitaxial films as well as TiO_2 anatase and TiO_2 rutile reference materials. (b) Experimental Ti K-shell extended X-ray absorption fine structure for epitaxial $Ti_{0.04}Fe_{1.96}O_3$ along with a simulation based on the optimized structure in which Ti substitutes for Fe.

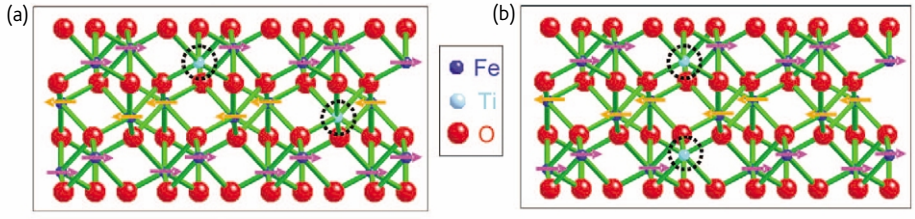

Fig. 6 Crystal structure diagrams for Ti:α-Fe_2O_3 in which Ti ions randomly occupy cation sites in both spin sublattices (a), or preferentially occupy sites in one spin sublattice (b). The dashed circles indicate the positions of substitutional Ti dopants.

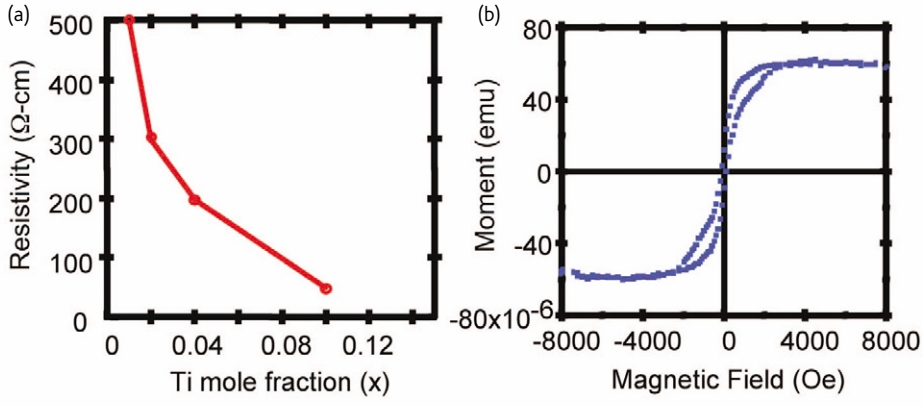

Fig. 7 (a) Resistivity versus Ti mole fraction (x) in $Ti_xFe_{2-x}O_3$. (b) In-plane magnetic hysteresis loop for $Ti_{0.07}Fe_{1.93}O_3$ measured at 300 K.

considered to be a magnetic 'undopant' because Ti(IV) is a d^0 system. When Ti(IV) substitutes for Fe(III) (a d^5 ion), 5 μ_B of magnetization is lost per Ti. Whether Ti doping results in net ferromagnetism depends on whether Ti substitutes randomly for Fe or preferentially occupies alternating cation layers along the *c*-axis. These two structures are shown in Fig. 6. In Fig. 6a, Ti is depicted as randomly occupying cation sites, displacing approximately equal numbers of Fe ions in adjacent layers. The spin moments of Fe ions in adjacent layers are oriented in approximately opposite directions at room temperature. Therefore, the in-plane magnetization is near zero for this configuration. However, if Ti dopants preferentially occupy alternating Fe bilayers, as they do in ilmenite ($FeTiO_3$), then a net magnetization should result, as depicted in Fig. 6b. Recent theoretical calculations predict that the ilmenite-like structure is more energetically favorable than the randomly doped structure[33,34]. In contrast, our DFT calculations[16] yield a total energy difference of only 0.038 eV between supercells of the two structures for $x = 0.04$, with substitution in both spin sublattices slightly more energetically favorable, but nevertheless predicting that one will not tend to preferentially nucleate over the other.

Looking next at the electrical properties, Fig. 7a reveals that the resistivity drops with increasing Ti concentration, but not to values expected if all Ti donor electrons are itinerant. This result suggests some degree of carrier localization, as discussed below. Fig. 7b shows a typical in-plane magnetic hysteresis curve taken at 300 K for a $Ti_{0.04}Fe_{1.96}O_3$ film that displays a saturation magnetization of ~0.5 μ_B/Ti. The saturation magnetization was found to range from 0.37-0.72 μ_B/Ti over many films of different *x*, and did not scale with *x*. This moment is a fraction of that expected if a ferromagnetically ordered, layered phase (Fig. 6b) had exclusively nucleated. At the same time, 0.5 μ_B/Ti exceeds what is expected if the Ti distribution was perfectly random (Fig. 6a). This result suggests that a minority (~1/8) of the Ti forms a ferromagnetically ordered phase, with the remainder being randomly distributed, which is consistent with high resolution

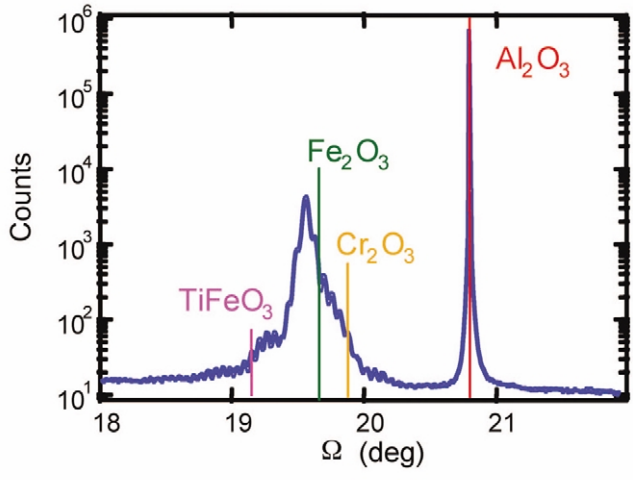

Fig. 8 High-resolution X-ray diffraction rocking curve measurement for 710Å $Ti_{0.04}Fe_{1.96}O_3$/130 Å Cr_2O_3/α-Al_2O_3(001).

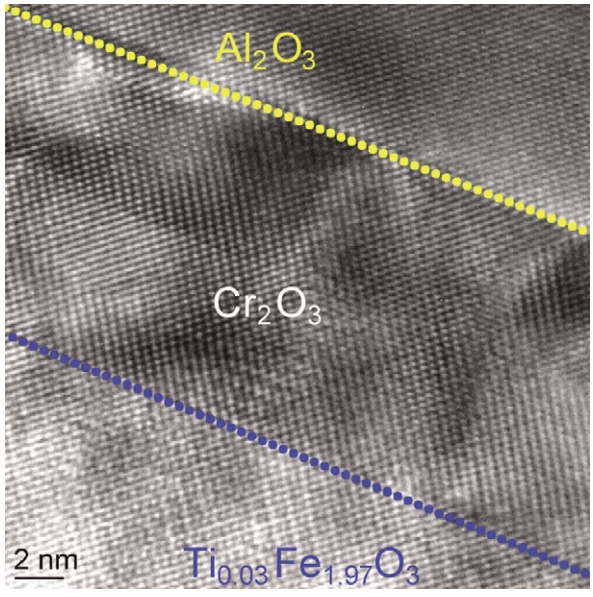

Fig. 9 High-resolution transmission electron microscopy lattice image for epitaxial $Ti_{0.03}Fe_{1.97}O_3/Cr_2O_3/\alpha\text{-}Al_2O_3(001)$.

X-ray diffraction, as seen in Fig. 8. Here, two distinct (006) Bragg peaks are visible at Ω = 19.5° and 20.8°. The latter is clearly associated with Al_2O_3, but the former is lower than the Bragg angle expected for pure Fe_2O_3 (19.7°). Weaker Bragg features appear to be present at Ω = ~19.8° and ~19.3° but they are masked by finite-thickness interference fringes or Laue oscillations. These two features are quite close to the Bragg angles expected for Cr_2O_3 and Ti:α-Fe_2O_3, the latter suggesting the presence of a $TiFe_2O_3$-like ordered minority phase along with randomly doped $Ti_xFe_{2-x}O_3$. Laue oscillations arising from the film peaks reveal that the crystalline quality is excellent throughout the entire thickness, as corroborated by transition electron microscopy (Fig. 9), and the low minimum yields in Rutherford backscattering spectrometry (RBS) (not shown). There is no indication of Ti or Fe interstitials in the RBS.

The conclusion of biphasic ordering is also supported by the fact that the magnetic hysteresis loops exhibit a dual-lobe structure (Fig. 7b), which is best interpreted as two microstructurally distinct regions. This dual-lobed hysteretic behavior has been seen previously in hematite-ilmenite solid solutions[35], and we suggest a similar explanation applies here. The dual lobes suggest the presence of two magnetic phases, one of high coercivity and one of low coercivity. This interpretation is supported by the fact that in-plane anisotropies measured at saturation and at ~75% of saturation (not shown) reveal different angular dependences. We suggest that the overall loop originates with the ilmenite-like phase, some of which contains antiphase boundaries. The low-coercivity portion of the loop results from coherent rotation, while the high-coercivity portion is caused by grain boundary domain wall pinning. Further testing of this hypothesis requires the correlation of local structure and composition by ultrahigh resolution scanning transmission electron microscopy (STEM) and high-resolution electron energy loss spectroscopy (EELS) with magnetic properties.

The persistence of high resistivity at large Ti doping levels results from donor electron localization on Fe sites, as seen in X-ray photoelectron core-level and valence band measurements. These are shown in Fig. 10. The Fe 2*p* core-level line shape is essentially identical to that for pure hematite for *x* = 0-0.08. Multiplet splitting and shake up associated with Fe(III) in a distorted octahedral field of O ligands, along with spin-orbit splitting, define the lineshape[36]. However, at *x* = 0.15, a weak peak characteristic of Fe(II) appears[37], resulting from localization of donor electrons on and the associated reduction of

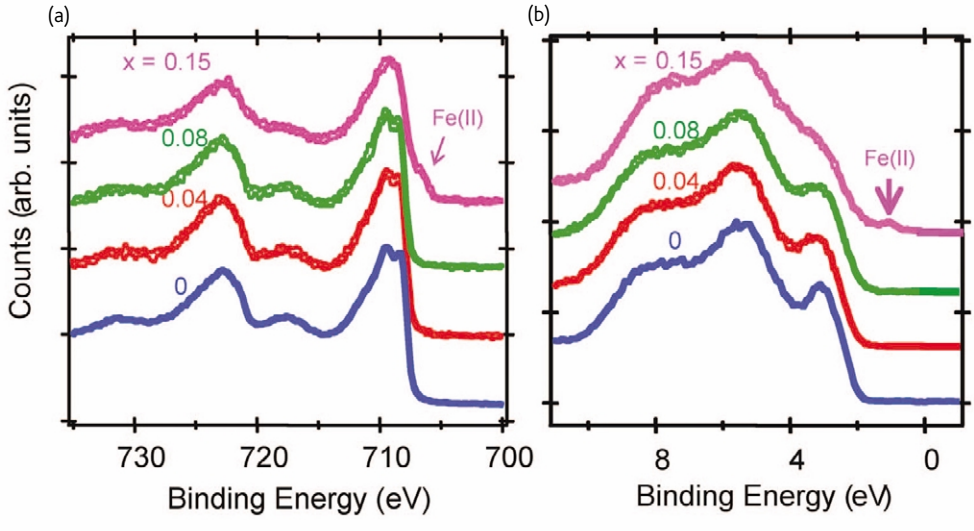

Fig. 10 High-resolution Fe 2p (a) and valence band (b) X-ray photoemission spectra versus x in epitaxial $Ti_xFe_{2-x}O_3$.

Fe(III) sites. A new feature also appears at midgap in the valence band spectrum at $x = 0.15$ corresponding to Fe(II)[38]. The extensive localization of donor electrons on Fe sites prevents the conductivity from reaching values characteristic of a highly doped semiconductor. Nevertheless, the material exhibits RTFM. Therefore, the ferromagnetic response appears to be a natural consequence of substitutional Ti at Fe lattice sites, independent of dopant-derived carriers. There is no systematic dependence of saturation moment on conductivity as x is varied.

Summary

In this brief review, we have described two systems, Co:ZnO and Ti:α-Fe_2O_3, that exhibit RTFM in the presence of donor electrons. In the case of Co:ZnO, donor electrons are introduced after growth by incorporating Zn_i, a shallow donor. The saturation magnetization is so strongly correlated with the Zn_i concentration that a cause-and-effect relationship between donor electrons and ferromagnetism is fully justified. True DMS behavior should manifest itself by relevant magnetotransport properties. Indeed, a very recent paper reveals magnetoresistive behavior near the metal-insulator transition in Co:ZnO films allegedly made *n*-type by Al doping[39]. In contrast, the unusual magnetic hysteresis exhibited by Ti:α-Fe_2O_3 is independent of donor electron concentration and appears to be a result of Ti(IV) substitution for Fe(III) in antiferromagnetic α-Fe_2O_3, leading to a spin imbalance in the cation sublattice. The magnitude of the saturation moment, as well as the unusual two-lobed hysteresis behavior, depend on the extent to which Ti dopants are distributed in a nonrandom way.

Returning to the question, "Is it possible to create magnetic semiconductors that work at room temperature?"[1], the answer is in the operative word 'works'. If by 'semiconductors that work' we mean semiconductors that enable the fabrication of spin-based devices that exhibit usefully large, gateable spin polarizations at room temperature, then we have more work to do. If, on the other hand, we mean semiconductors that exhibit a dependence of magnetization on carrier concentration, then tantalizing results are emerging for *n*-Co:ZnO. However, we still have more work ahead of us as we strive to optimize the materials properties, develop new materials, gain deeper understanding and fabricate elementary devices, such as the spin-LED, that work at and above room temperature. mt

Acknowledgments

This work was funded by the US Department of Energy (DOE) Office of Science Division of Materials Sciences and Engineering, the US National Science Foundation (DMR-0239325 to DRG), the Research Corporation, the Dreyfus Foundation, and the Sloan Foundation. KMR gratefully acknowledges support from the Geosciences Division of the DOE Office of Basic Energy Sciences and from the Office of Biological and Environmental Research through the Stanford Environmental Molecular Sciences Institute. Some of the work was carried out at the Environmental Molecular Sciences Laboratory (a national scientific user facility sponsored by the US DOE Office of Biological and Environmental Research and located at Pacific Northwest National Laboratory). Use of the Advanced Photon Source was supported by the US DOE under Contract No. W-31-109-ENG-38.

REFERENCES

1. Kennedy, D., and Norman, C., *Science* (2005) **309**, 82
2. Nazmul, A. M., *et al.*, (2002) *cond-mat.* 0208299
3. Dietl, T., *et al.*, *Science* (2000) **287**, 1019
4. Dietl, T., *et al.*, *Phys. Rev. B* (2001) **63**, 195205
5. Prellier, W., *et al.*, *J. Phys.: Condens. Matter* (2003) **15**, R1583
6. Janisch, R., *et al.*, *J. Phys.: Condens. Matter* (2005) **17**, R657
7. Liu, C., *et al.*, *J. Mater. Sci.* (2005) **16**, 555
8. Fukumura, T., *et al.*, *Semicond. Sci. Technol.* (2005) **20**, S103
9. Chambers, S. A., *Surf. Sci. Rep.* (2006) **61**, 345
10. Claflin, B., *et al.*, *J. Cryst. Growth* (2006) **287**, 16
11. Kittilstved, K. R., *et al.*, *Nat. Mater.* (2006) **5**, 291
12. Chambers, S. A., *et al.*, *Appl. Phys. Mater. Sci. Process.* (2006), in press
13. Xu, H. Y., *et al.*, *Appl. Phys. Lett.* (2006) **88**, 242502
14. Sato, K., and Katayama-Yoshida, H., *Semicond. Sci. Technol.* (2002) **17**, 367
15. Kittilstved, K. R., *et al.*, *Appl. Phys. Lett.* (2006) **89**, 062510; *cond-mat*/0507121
16. Droubay, T. C., *et al.*, *Phys. Rev. B* (2006), submitted
17. Ohno, H., *et al.*, *Nature* (1999) **402**, 790
18. Chye, Y., *et al.*, *Phys. Rev. B* (2002) **66,** 201301
19. Van Dorpe, P., *et al.*, *Appl. Phys. Lett.* (2004) **84,** 3495
20. Buyanova, I. A., *et al.*, *J. Vac. Sci. Technol. B* (2006) **24**, 259
21. Schwartz, D. A., and Gamelin, D. R., *Adv. Mater.* (2004) **16**, 2115
22. Tuan, A. C., *et al.*, *Phys. Rev. B* (2004) **70**, 054424
23. Shim, M., and Guyot-Sionnest, P., *Nature* (2000) **407**, 981
24. Kittilstved, K. R., *et al.*, *Phys. Rev. Lett.* (2006) **97**, 037203
25. Gebhardt, E., *Z. Mattlk* (1947) **37**, 87
26. Moore, W. J., and Lee, J. K., *Trans. Faraday Soc.* (1951) **47**, 501
27. Secco, E. A., *J. Chem. Phys.* (1958) **29**, 406
28. Coey, J. M. D., *et al.*, *Nat. Mater.* (2005) **4**, 173
29. Kacman, P., *Semicond. Sci. Technol.* (2001) **16**, R25
30. Torrance, J. B., *et al.*, *Phys. Rev. Lett.* (1972) **29**, 1168
31. Coey, J. M. D., *et al.*, *Appl. Phys. Lett.* (2004) **84**, 1332
32. Chambers, S. A., *et al.*, *Phys. Rev. B* (2000) **61**, 13223
33. Butler, W. H., *et al.*, *J. Appl. Phys.* (2003) **93**, 7882
34. Bandyopadhyay, A., *et al.*, *Phys. Rev. B* (2004) **69**, 174429
35. Carmichael, C. M., *Proc. R. Soc. London, A* (1961) **263**, 508
36. Droubay, T. C., and Chambers, S. A., *Phys. Rev. B* (2001) **64**, 205414
37. Chambers, S. A., *et al.*, *Surf. Sci.* (2000) **450**, L273
38. Lad, R. J., and Henrich, V. E., *Phys. Rev. B* (1989) **39,** 13478
39. Xu, Q., et al., *Phys. Rev. B* (2006) **73**, 205342